

RSC Advances



This is an *Accepted Manuscript*, which has been through the Royal Society of Chemistry peer review process and has been accepted for publication.

Accepted Manuscripts are published online shortly after acceptance, before technical editing, formatting and proof reading. Using this free service, authors can make their results available to the community, in citable form, before we publish the edited article. This *Accepted Manuscript* will be replaced by the edited, formatted and paginated article as soon as this is available.

You can find more information about *Accepted Manuscripts* in the [Information for Authors](#).

Please note that technical editing may introduce minor changes to the text and/or graphics, which may alter content. The journal's standard [Terms & Conditions](#) and the [Ethical guidelines](#) still apply. In no event shall the Royal Society of Chemistry be held responsible for any errors or omissions in this *Accepted Manuscript* or any consequences arising from the use of any information it contains.

Molecular insights into the damping mechanism of Poly(vinyl acetate)/hindered phenol hybrids by a combination of experiment and molecular dynamics simulation

Kangming Xu, Fengshun Zhang, Xianglong Zhang, Jiwei Guo, Hong Wu*, Shaoyun Guo*

State Key Laboratory of Polymer Materials Engineering, Polymer Research Institute of Sichuan University, Chengdu, Sichuan 610065, China

ABSTRACT

The fundamental mechanism of the improved damping properties of poly(vinyl acetate) (PVAc) contributed by the introduction of hindered phenol was systematically elucidated by two-dimensional infrared (2D IR) spectroscopy, dynamic mechanical analysis (DMA), differential scanning calorimeter (DSC), X-ray diffraction (XRD) and molecular dynamics (MD) simulation. 2D IR results revealed the hydrogen bonds (H-bonds) evolution from intermolecular H-bonds to H-bonds network of PVAc/hindered phenol. Subsequent DMA results revealed that the damping properties of PVAc exhibited two different degrees of the improvement due to the addition of hindered phenol. Meanwhile, DSC results showed that all hybrids were miscible as concentration fluctuations change irregularly. According to the XRD observation of only amorphous hindered phenol existing in PVAc matrix, further MD simulation, based on an amorphous cell, characterized the number of H-bonds, the binding energy and the fractional free volume (FFV) of the hybrids. It was observed that the variation tendency of the simulation data was in accordance with the experimental results.

* Corresponding authors: E-mail: wh@scu.edu.cn; nic7702@scu.edu.cn;
Tel/fax:: +86-28-85466077; +86-28-85405135

Therefore, the damping mechanism of PVAc/hindered phenol hybrids was proposed through a detailed analysis on the synergy effects of the number of intermolecular H-bonds and binding energy between PVAc and hindered phenol as well as the FFV or dynamic heterogeneity.

Keywords: Poly(vinyl acetate); Hindered phenol; Damping mechanism; Molecular dynamics simulation; Two-dimensional infrared spectroscopy.

1. INTRODUCTION

Airborne noise and structural vibration control nowadays has become a fundamental concern in both industries and our daily life. Viscoelastic polymers with the capacity of reducing unwanted noise and preventing vibration fatigue failure, therefore, have been widely used for acoustic and vibration damping [1]. The damping mechanism of the polymer is a reaction of internal friction [2]. When the chain segments in a polymer backbone make de Gennes-like reptation motions [3], molecular vibrational energy is converted into heat energy, thus a loss peak appears in a certain temperature range from the dynamic mechanical results. According to the damping theory [4-6], the height and width of the loss peak are mutually linked. As a result, a loss peak, which is both high and wide at the same time, is unavailable for a homopolymer. However, in order to meet the requirements for applications, damping polymer materials should exhibit a high loss peak in a wide range. Therefore, efforts have been made to solve the issue by different methods, such as blending [7], co-polymerization [8], interpenetration networks (IPN) polymers [9] and gradient

polymers [10], as well as the main concern of this paper: The use of hydrogen bonds (H-bonds) for the design of damping hybrids or so-called "self-assembled" materials.

During recent years, many efforts have been devoted to improving damping properties of polymer hybrids through H-bonds and exploring its mechanism. For example, rubber/hindered phenol or hindered amine such as tetrakis[methylene-3-(3-5-di-tetra-butyl-4-hydroxy phenyl) propionyloxy]methane (AO-60) [11], triethylene glycolbis-[3-(3-tertbutyl-4-hydroxy-5-methyl phenyl)propionyloxy] (AO-70) [11], 3,9-bis[1,1-dimethyl-2-{b-(3-tert-butyl-4-hydroxy-5-methylphenyl)propionyloxy}-ethyl]-2,4,8,10-tetraoxaspiro[5,5]-undecane (AO-80) [12], 2,20-methylene bis(6-tert-butyl-4-methylphenol) (AO-2246) [13], and N,N-dicyclohexyl-2-benzothiazolylsulfenamide (DZ) [14] have been widely investigated as a type of high performance damping material [15]. Moreover, in order to explore the damping mechanism in the hybrids, Zhao et al. first investigate the damping mechanism of the nitrile-butadiene rubber (NBR)/AO-80 hybrids in a quantitative manner with the help of molecular dynamics (MD) simulation and attribute the cause of maximum dynamic property to the largest number of H-bonds and the greatest binding energy as well as the minimum fractional free volume (FFV) by a combination with the experimental results [16]. Subsequently, Song et al. also propose a similar conclusion by the combination of MD simulation and experimental results of NBR/AO-60 hybrids [17]. However, to our surprise, though the polymers with glass transition temperature (T_g) above ambient temperature play an important role in damping material fields, the

H-bonds predominant damping mechanism in these polymer/hindered phenol systems have been hitherto rarely reported. And though the H-bond damping mechanism of polymer/ hinder phenol hybrids had been widely studied, some mechanisms were still unclear, For example, the effect of the intramolecular H-bonds to the damping properties was not well understood yet. Therefore, in order to fabricate the composites with high damping properties, it is necessary to investigate the formation mechanism of H-bonds in T_g above ambient temperature polymer/hindered phenol hybrids and their effects on the damping behavior of the hybrids.

To characterize structural and spectroscopic properties related to H-bonds, two of the most useful approaches are infrared spectroscopy, in particular, two-dimensional infrared (2D IR) spectroscopy [18-22] and MD simulations [23, 24]. It is widely accepted that the formation of the H-bond X-H...Y results in weakening both the bond of X-H and the bond adjacent to Y, thus leads to the decrease of vibration frequencies of X-H and Y species. The decreased frequency can be detected by IR spectroscopy, which provides unambiguous information about the formation of H-bonds. However, in some special cases, certain useful information on H-bonds could not be easily “decoded” from the overlapped conventional IR spectral analysis. 2D IR correlation spectroscopy can extract information that cannot be obtained straight from one-dimensional spectroscopy, since the spectral resolution can be enhanced by spreading peaks along the second dimension [25-28]. Therefore, 2D IR correlation spectroscopy has become a powerful and versatile tool for elucidating subtle spectral changes induced by an external perturbation. On the other hand, MD

simulation provides one of the most direct ways to theoretically investigate the molecular behavior [29], which is not accessible to experimental approaches in complex systems, such as a system involving H-bond interactions [30]. Furthermore, in order to obtain useful insight into the H-bond dynamics, it is important to establish the correlation between the simulation results of structural or vibrational properties and experimental measurement results [31].

Therefore, to investigate the detailed H-bonds predominant damping mechanism in viscoelastic polymer/hindered phenol hybrids, Poly(vinyl acetate) (PVAc), with hydroxyl side group acting as proton acceptor, is selected as the matrix in this paper. It is a typical amorphous and polar polymer with a T_g above ambient temperature, which is easy processing and has been commonly used as damping materials, such as the use as backing material in loudspeaker production for damping noise vibration [32]. AO-70, with two hydroxyl end groups acting as proton donor, is added into PVAc for the purpose to obtain high damping hybrids. Furthermore, with the combination of experiment and MD simulation, the relationship between the H-bonds structures and the damping properties of PVAc/AO-70 hybrids is detailed interpreted.

2. EXPERIMENTAL AND SIMULATION STRATEGIES

2.1 Materials

Poly(vinyl acetate) (PVAc) (grade G30) with a molecular weight of 4×10^4 - 6×10^4 g/mol and a solids content of 100% was purchased from Wuxi Sincere Chemicals Co., Ltd. (Wuxi, China). Triethylene glycolbis-[3-(3-tertbutyl-4-hydroxy-5-methyl

phenyl)propionyloxy] (AO-70 or KY-2080), in powder form, was obtained from Beijing Additive Research Institute (Beijing, China). Tetrahydrofuran (analytical grade) was purchased from Chengdu Kelong Chemical Reagent Factory (Chengdu, China). All materials were used without further purification and the molecular structure of PVAc and AO-70 were showed in Figure 1.

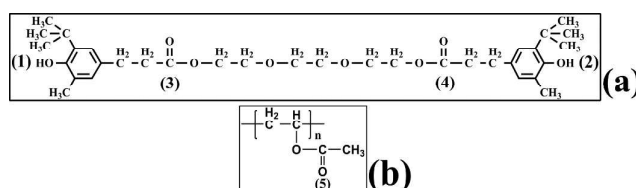


Figure 1. Molecular structures of (a) AO-70 and (b) PVAc.

2.2 sample preparation

PVAc/AO-70 binary hybrids were prepared as follows: (1) The as-received PVAc and AO-70 were dried in a vacuum oven at 50 °C for 24 h. (2) The dried PVAc was first hot sheared in a Haake internal mixer (Rheocord 90, Germany) at a rotor speed of 30 rpm for 1 min at 120 °C. (3) AO-70 powders with weight ratios of 0 phr, 6.25 phr, 12.5 phr, 25 phr, 37.5 phr and 50 phr were added to the sheared PVAc, respectively. (4) The mixtures were mixed in the Haake internal mixer at a rotor speed of 60 rpm for another 8 min at 120 °C to prepare the binary hybrids. These are designated, respectively as PVAO-0 phr to PVAO-50 phr.

In order to get mixed samples for characterization, the hybrids were first dried at 60 °C for 12 h, then preheated at 120 °C for 10 min, hot-pressed at 120 °C for 5 min under 12 MPa, and then cool-pressed at room temperature under 12 MPa.

2.3 Characterization

2.3.1 Fourier Transform Infrared Spectroscopy (FTIR)

The temperature-dependent absorbance FTIR spectra of PVAc, AO-70 and the hybrids were recorded with a 2 cm^{-1} spectral resolution on a Nicolet-IS10 (Thermo Electron Co., USA) spectrometer by signal averaging 20 scans. Two pieces of microscope KBr windows, which have no absorption bands in the MIR region, were used to prepare a transmission cell. Variable-temperature spectra, controlled by a temperature control instrument including a programmed heating cell and a circulating water jacket cooling system, were collected between 20 and 120 °C with an increment of 5 °C. All samples were prepared via solvent casting from 20 g/L tetrahydrofuran solution, dried in a vacuum oven at 60 °C for 12 h and protected by dried high-purity Nitrogen gas during the measurement. The baseline correct processing was performed by the automatic baseline correction of OMNIC 8.2 spectral collecting software (Thermo Fisher Scientific Inc., USA).

2.3.2 Two-Dimensional (2D) Correlation Analysis

Spectra recorded at an interval of approximately 10 °C were selected in certain wavenumber ranges and the generalized 2D correlation analysis was applied by the 2D Shige software composed by Shigeaki Morita (Kwansei-Gakuin University, Japan). In the 2D correlation maps, the red regions are defined as the positive correlation intensities, whereas the blue ones are regarded as the negative correlation intensities.

2.3.3 Dynamic mechanical analysis (DMA)

Dynamic mechanical spectra were acquired through a dynamic mechanical analyzer (Q800, TA Instrument). The samples with sizes of 10 mm (length) \times 10 mm (width) \times 1 mm (thickness) were heated from -20 to 100 °C at a constant frequency of 10 Hz with controlled stress by 0.1% and a heating rate of 3 °C /min under a single-cantilever mode.

2.3.4 Differential scanning calorimetry (DSC)

The thermal properties of PVAc, AO-70, and the hybrids (5–7 mg) were measured using differential scanning calorimetry (Q20, TA Instrument). The Nitrogen gas was purged throughout the measurements. The sample was first heated from room temperature to 120 °C (first heating) to eliminate heat history. Subsequently, the sample was cooled to -50 °C and heated again to 120 °C (second heating). All the heating and cooling rates were 10 °C/min. The glass transition temperature (T_g) were obtained from the second heating scan. The melting temperature (T_m) of the as-received AO-70 was obtained from the first heating scan.

2.3.5 Wide-angle X-ray diffraction (WXR)

WXR measurements were performed on an X'Pert Pro X-ray diffractometer (Philips) using Cu $K\alpha$ radiation ($\lambda = 0.154$ nm, 40 kV, 40 mA) at room temperature. The scanning rate was 8 °/min.

2.3.6 Ultraviolet spectroscopy (UV)

The UV spectra of the PVAc, AO-70, and the hybrids were obtained with a

Shimadzu 1705 UV-visible spectrophotometer. The wavelength ranged from 200 to 1100 nm at a resolution of 1 nm. The linear correlation coefficient is greater than 0.999.

2.4 Simulation Strategies for PVAc/AO-70 hybrids

MD simulation had been performed on the PVAc/AO-70 hybrids at ambient temperature (25 °C) using the software packages of Discover and Amorphous cell modules (Accelrys, Inc., San Diego, CA) with the Material Studio Modeling (version 5.0). The COMPASS (condensed-phase optimized molecular potentials for atomistic simulation studies) force field, which was used for computing interatomic interactions, has been widely used to optimize and predict the structural, conformational, and thermophysical condensed phase properties of the molecules including polymers [33]. In the COMPASS force field approach, total energy, E_T of the system is represented by the sum of bonding and nonbonding interactions given as the following:

$$E_T = E_b + E_o + E_\phi + E_{loop} + E_{pe} + E_{vdw} + E_q \quad (1)$$

Here, the first five terms represent the bonded interactions, which correspond to energies associated with the bond, E_b ; bond angle bending, E_o ; torsion angle rotations, E_ϕ ; out of loop, E_{loop} ; and potential energy, E_{pe} . The last two terms represent nonbonded interactions, which consist of van der Waals term, E_{vdw} , and electrostatic force, E_q [34]. Initial velocities were set by using the Maxwell-Boltzmann profiles at 25 °C. The verlet velocity time integration method was used with the time step of 1 femtosecond (fs) [35].

Using the rotational isomeric state (RIS) theory that describes the conformations of unperturbed chains, initially the structures of AO-70 and PVAc polymer chain containing 50 repeat units [36] were built and energy-minimized. The lengths of the chain repeat units were chosen according to two criteria: (1) to keep cell size and computing time at a manageable level (one long chain would be a less realistic option than a few short chain) and (2) to ensure sufficient mobility of chain to allow chain movements within the modelling time period [16]. Cubic amorphous cells containing 4 PVAc polymer chains and different mass ratio AO-70 as Table 1 showed were constructed with the periodic boundary condition applied. The density of MD simulation and experimental results are also summarized in Table 1. The agreement of the simulated densities with the experimental values ($\rho_{\text{MD}} - \rho_{\text{Exp}} < 0.004$) indicated that the motion of the polymer chains in the hybrids can be expressed by MD simulation.

Table 1. Mass ratio and density of PVAc/AO-70 hybrids by experiment and MD simulation.

Sample Name	PVAO-0 phr	PVAO-6.25 phr	PVAO-12.5 phr	PVAO-25 phr	PVAO-37.5 phr	PVAO-50 phr
Experiment mass ratio* (phr)		9.45	13.85	28.19	39.23	50.71
MD simulation mass ratio (phr)		10.22	13.62	27.24	40.86	51.08
Experiment Density (g/cm³)	1.1880	1.1829	1.1807	1.1741	1.1666	1.1575
MD simulation density (g/cm³)	1.1902	1.1825	1.1802	1.1703	1.1635	1.1565

* Experiment mass ratio was obtained from the UV results.

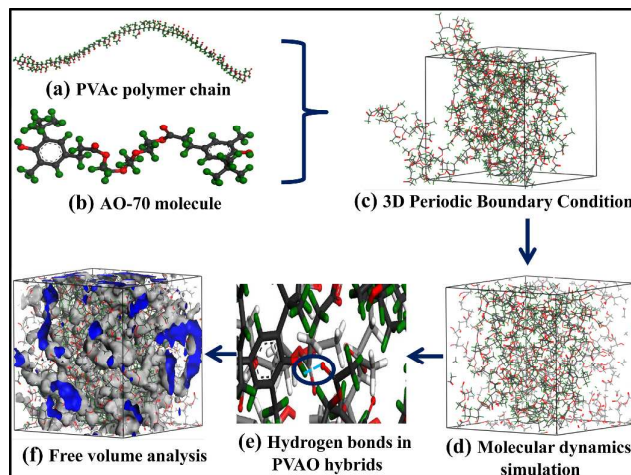


Figure 2. Models for MD simulation of PVAO hybrids (red atom is O, green atom is H, grey atom is C, and blue dashed line represents H-bonds).

Figure 2 shows the process of MD simulation. After the construction of the amorphous cells (Figure 2(a)-(c)), the total system was energy-minimized with the steepest descent method followed by the conjugate gradient method. Subsequently, in order to adjust the periodic box size and to obtain an energy equilibrated cell, the cell was equilibrated in the isothermal-isobaric (NPT) ensemble at 1 atm and 25 °C. This equilibration was done for 1 nanosecond (ns) with the dynamics that was followed by the data accumulation running for another 1 ns and the configurations saved for every 5 picosecond (ps) (Figure 2(d)). Finally, the cell could be used to count the number of H-bonds (Figure 2(e)) and to analyze the FFV (Figure 2(f)) as well as the binding energy. The FFV of the equilibrated hybrids was determined by a grid scanning method.

3. RESULTS AND DISCUSSION

3.1 Hydrogen bonds in PVAO hybrids

Combined with the chemical structures of AO-70 and PVAc shown in Figure 1, Multiple H-bonds might be formed between one type of proton donator (phenolic O-H groups in AO-70 (Figure 1(1)(2))) and two types of proton acceptors (ester C=O groups in both PVAc (Figure 1(5)) and AO-70 (Figure 1(3)(4))) in PVAO hybrids. To confirm the existence of the aforementioned H-bonds, temperature-dependent IR in the O-H, and C=O group regions of AO-70 and PVAO-50 phr were characterized and the results were shown in Figure 3.

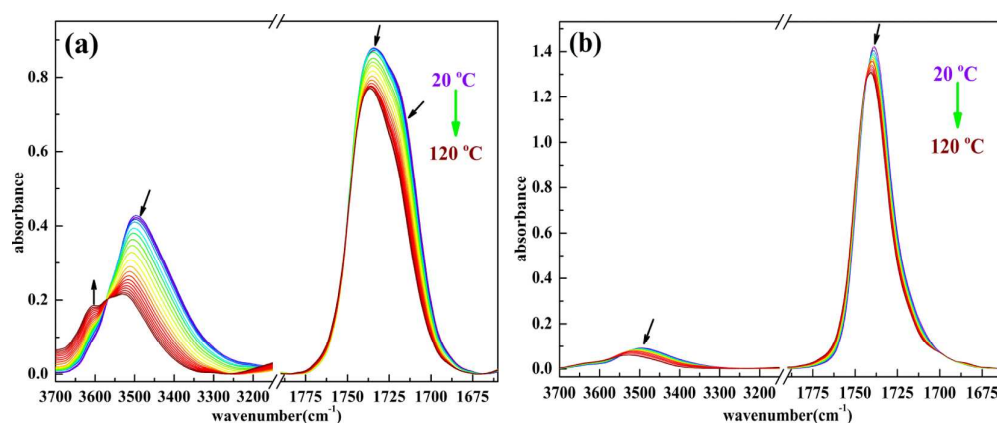


Figure 3. The temperature-dependent infrared spectrum of (a) AO-70 and (b) PVAO-50 phr in the range of 3700-3150 cm^{-1} and 1780-1660 cm^{-1} from 20 to 120 $^{\circ}\text{C}$.

It was well accepted that temperature played an important role in determining the extent of H-bonds. In general, the strength of H-bonds decreased with increasing temperature, resulting in the decreased intensity and the increased wavenumber of H-bonded IR peaks. For pure AO-70 (Figure 3(a)), the peak at 3480 cm^{-1} decreased and shifted to higher wavenumber while a new peak at 3590 cm^{-1} stood out with increasing temperature, which could be attributed to the vibration of H-bonded O-H and free O-H, respectively. Meanwhile, a distinct peak at 1735 cm^{-1} and a latent

shoulder peak at 1710 cm^{-1} both decreased and shifted to higher wavenumber with increasing temperature, which were corresponding to the vibration of free C=O and H-bonded C=O, respectively. Therefore, the H-bonded phenolic O-H/ester C=O were shown to exist in AO-70. However, for PVAO-50 phr (Figure 3(b)), only the decreased peak at 3480 and 1735 cm^{-1} , corresponding to the vibration of H-bonded O-H and free C=O, respectively, could be observed with increasing temperature. As a result, one might come up with the following questions: (1) where was the peak location of the H-bonded C=O and (2) what kind of H-bond was formed in PVAO hybrids, intermolecular, intramolecular or the both? In order to check out the latent peaks in C=O region and make clear H-bond relationship in PVAO hybrids, 2D IR, with higher sensitivity, was applied. And the results were shown below. The results for AO-70 and PVAO-6.25 phr were also taken into account for a comparison.

2D IR correlation spectra were characterized by two independent wavenumber axes (ν_1 , ν_2) and a correlation intensity axis. Two types of spectra, 2D synchronous and asynchronous spectrum, were obtained in general. In the synchronous spectra, diagonal positive peaks were referred to as autopeaks, which represented the overall extent of the temperature-induced fluctuation of spectral intensity with respect to the reference spectrum. The off-diagonal peaks were called crosspeaks and their presence indicated that the simultaneous changes occurred at two different wavenumbers. Positive crosspeaks demonstrated that the intensity variations of the two peaks at ν_1 and ν_2 were taking place in the same direction (both increase or both decrease) under the environmental perturbation, while the negative cross-peaks helped to infer that the

intensities of the two peaks at ν_1 and ν_2 change in opposite directions (one increases, while the other one decreases) under perturbation. The asynchronous spectra had only off-diagonal peaks. The intensity of the asynchronous spectrum represented sequential or successive changes of spectral intensities observed at ν_1 and ν_2 . A positive asynchronous peak at (ν_1, ν_2) implied that the intensity at ν_1 changed faster compared to that at ν_2 , while the negative asynchronous peak implied the opposite phenomenon. And this feature is very useful in differentiating overlapped or latent peaks due to different spectral origin [37].

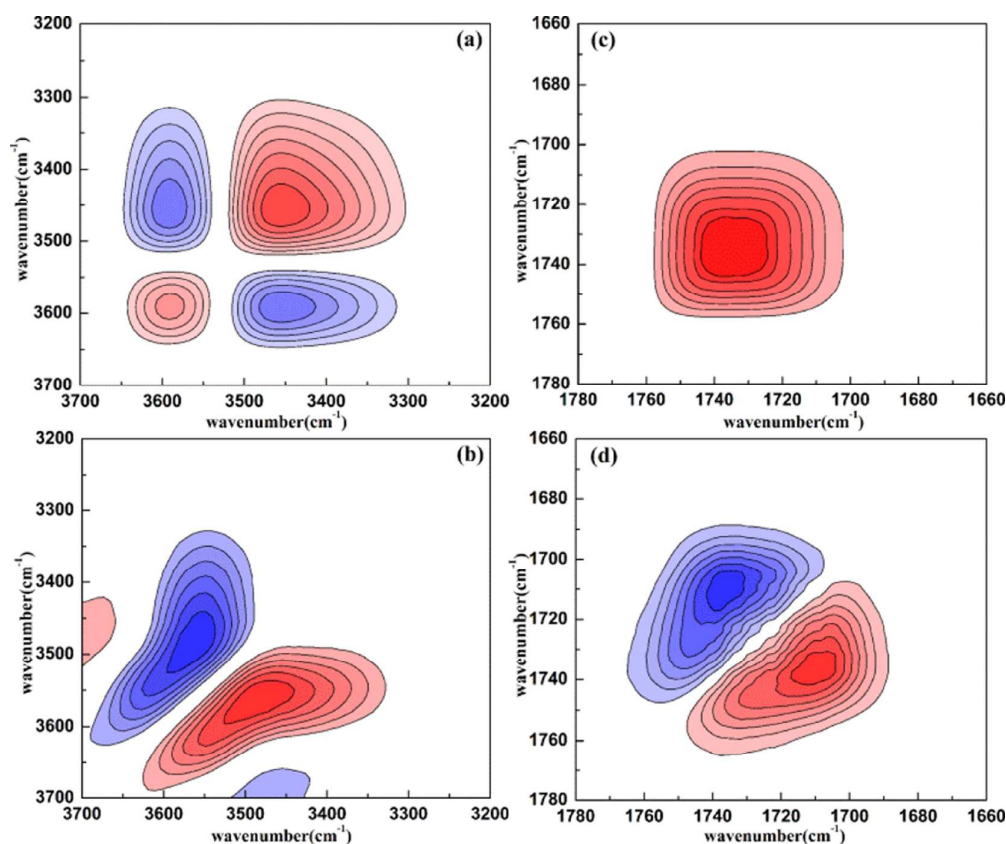


Figure 4. 2D IR correlation spectra of AO-70 obtained from 20 to 120 °C: (a) synchronous map of 3700-3200 cm⁻¹, (b) asynchronous map of 3700-3200 cm⁻¹, (c) synchronous map of 1780-1660 cm⁻¹ and (d) asynchronous map of 1780-1660 cm⁻¹.

The synchronous and asynchronous maps for the heating process of AO-70 in the 3700-3200 cm^{-1} and 1780-1660 cm^{-1} region are shown in Figure 4. In the synchronous map of 3700-3200 cm^{-1} (Figure 4(a)), two strong autopeaks developed at 3590 and 3480 cm^{-1} , indicating the prominent changes of free and H-bonded O-H with increasing temperature. The negative crosspeaks showed that the heating induced intensity variations of the peaks at 3590 and 3480 cm^{-1} were simultaneously changed in an opposite direction. In the asynchronous map of 3700-3200 cm^{-1} (Figure 4(b)), the crosspeak implied that out-of phase spectral changes occurred at 3590 and 3480 cm^{-1} . The synchronous spectrum (Figure 4(c)) in the 1780-1660 cm^{-1} range was dominated by only one strong autopeak at 1735 cm^{-1} , which was attributed to the vibration of free C=O with increasing temperature. According to the crosspeaks in the asynchronous map of 1780-1660 cm^{-1} (Figure 4(d)), the existence of the peak at 1710 cm^{-1} , attributed to the vibration of H-bonded C=O, could be detected. Therefore, it was confirmed that the results of the above 2D IR analysis were well consistent with that of the temperature-dependent FTIR.

2D IR maps of PVAO-6.25 phr and PVAO-50 phr are depicted in supporting information (Figure 1-S and Figure 2-S, respectively). For PVAO-6.25 phr, in the synchronous maps of O-H and C=O region,, two autopeaks developed at 3590 and 1735 cm^{-1} , indicating the prominent changes of them with increasing temperature. In the asynchronous map of O-H group region, two symmetrical crosspeaks confirmed the presence of free and H-bonded O-H groups at 3590 and 3480 cm^{-1} , respectively. In the asynchronous map of C=O group region, the presence of two peaks (1735 and

1723 cm^{-1}) could be distinguished, which were assigned to the vibration of free and H-bonded C=O group, respectively. Therefore, by a comparison with AO-70, it could be concluded that the intermolecular H-bonds between PVAc and AO-70 were formed while no intramolecular H-bonds were detected in PVAO-6.25 phr. While with adding 50 phr AO-70 into PVAc, in the synchronous maps of O-H and C=O region, the autopeak developing at 3480, 1723 and 1735 cm^{-1} pointed out great changes of H-bonded O-H, C=O and free C=O with increasing temperature, respectively. And the negative crosspeak supported that the heating induced intensity variations of the peaks at 3480 and 3590 as well as 1723 and 1735 cm^{-1} were taking place in the opposite direction. In the asynchronous map of O-H region, the two symmetrical crosspeaks implied that out-of phase spectral changes occurred at 3590 and 3480 cm^{-1} . And in the asynchronous map of C=O region, three peaks (1735, 1723 and 1710 cm^{-1}) could be distinguished. Compared with AO-70 and PVAO-6.25 phr, the peak at 1723 cm^{-1} could be assigned to the vibration of intermolecular H-bonded C=O between PVAc and AO-70 while the peak at 1710 cm^{-1} could be attributed to the intramolecular H-bonded C=O of AO-70 itself.

Therefore, based on the 2D IR analysis, the schematic diagram of H-bonds in PVAO hybrids was put forward and shown in Figure 5. When small amount of AO-70 were added into PVAc, the H-bonds between O-H groups of AO-70 and C=O groups of PVAc were only formed in the hybrids. However, with adding more AO-70 into PVAc, the intramolecular H-bonds between O-H and C=O groups of AO-70 were coexisted with the intermolecular H-bonds between AO-70 and PVAc. Thus an

H-bond network was formed in the hybrids with high amount AO-70.

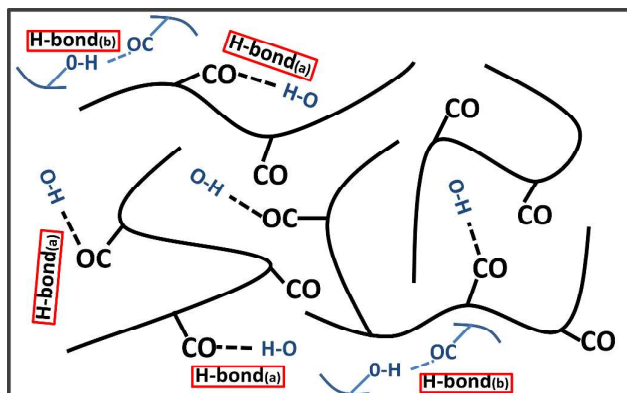


Figure 5. Schematic diagram of intermolecular H-bond (H-bond(a)) and intramolecular H-bond (H-bond(b)) in hybrids with black thick lines, blue short lines and black dashed lines denoting PVAc polymer chains, AO-70 small molecules, and H-bonds, respectively.

3.2 Dynamic mechanical analysis

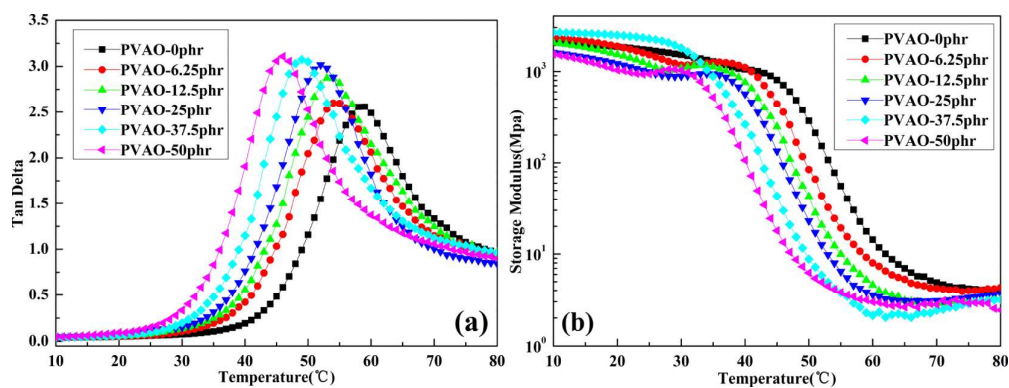


Figure 6. Temperature dependence of (a) loss factor ($\tan\delta$) and (b) storage modulus of PVAO hybrids.

Table 2. Temperature-loss factor values of PVAO hybrids.

Sample Name	Maximum value of Loss factor		Temperature Range of Loss factor greater than 1		
	Value	T/°C	T1/°C	T2/°C	$\Delta T/^\circ\text{C}$
PVAO-0 phr	2.564	58.80	49.08	77.67	28.59
PVAO-6.25 phr	2.618	55.21	44.84	76.27	31.43
PVAO-12.5 phr	2.891	53.64	43.28	79.45	36.17
PVAO-25 phr	3.032	52.15	41.75	78.54	36.79
PVAO-37.5 phr	3.086	48.72	39.19	77.05	37.86
PVAO-50 phr	3.129	46.14	36.10	74.06	37.96

As mentioned above, H-bonds play an important role in determining the damping properties of hybrids containing hindered phenol. To explore the effect of H-bonds evolution on the damping properties of PVAO hybrids, the temperature dependence of the loss factor ($\tan\delta$) and the storage modulus of the hybrids are depicted and the results are shown in Figure 6. The detailed DMA results are also summarized in Table 2. For DMA results, high value of $\tan\delta$ and wide temperature range of $\tan\delta$ greater than a constant value mean good damping properties of the material. For PVAO hybrids (Figure 6(a)), on the one hand, the only $\tan\delta$ peak, corresponding to the T_g of PVAc, gradually shifted to lower temperature with increasing the amount of AO-70, indicating that AO-70 had plasticizing effects on PVAc. For example, compared with pure PVAc had a T_g at about 60 °C, the T_g of PVAO-50 phr shifted almost 15 °C to about 45 °C, which was benefit for damping materials because the use temperature of damping materials was usually near ambient temperature. On the other hand, the maximum value of $\tan\delta$ and the value of temperature range of $\tan\delta$ greater than 1 increased with increasing the amount of AO-70 (Figure 6(a) and Table 2), which showed that AO-70 could effectively improve the damping properties of PVAc. However, the improvement could be divided into two stages. For the maximum value

of $\tan\delta$, the value increased rapidly with increasing the amount of AO-70 from 0 to 25 phr, whereas the value showed a slight increase with increasing further the amount of AO-70. The value of temperature range of $\tan\delta$ greater than 1 showed a similar trend with the maximum value of $\tan\delta$, too. Related to the H-bonds evolution in PVAO hybrids, the different improvements could be reasonably attributed to the intermolecular and intramolecular H-bonds changes in the hybrids. The storage modulus indicates the capability of a material to store mechanical energy and resist deformation. The loss of storage modulus from low temperature to high temperature may indicate the secondary transition and the glass transition of a polymer, respectively. In Figure 6(b), every storage modulus curve displayed two transitions corresponding to the movement of the side groups of PVAc (the lower temperature one) and the PVAc polymer chain (the higher temperature one) except for PVAO-37.5 phr, where only the glass transition corresponding to the movement of the PVAc polymer chain could be observed. The value of storage modulus in the low temperature region (before the glass transition) also gradually decreased with the increasing amount of AO-70 except for PVAO-37.5 phr, which exhibit the maximum value of storage modulus. All of these phenomena could also be reasonably attributed to the H-bonds evolution in the hybrids, especially the changes of intramolecular and intermolecular H-bonds. In order to explore the H-bond predominant damping mechanism in the hybrids, the quantitative analysis of the H-bonds evolution by molecular dynamics simulation were given in the following part, where the number of H-bonds, the binding energy and the fractional free volume would be discussed.

3.3 Compatibility and microstructure

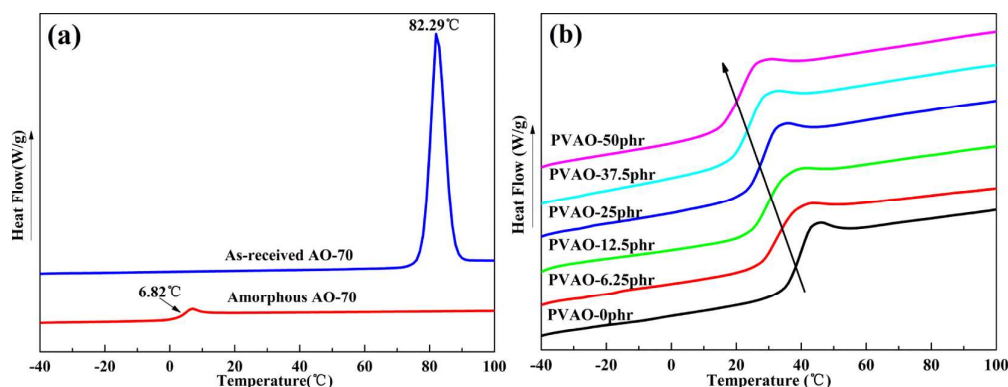


Figure 7. DSC curves of (a) AO-70 and (b) PVAO hybrids.

To further confirm the T_g variation observed above and to investigate the compatibility in the hybrids, the DSC traces of AO-70 and PVAO hybrids were obtained and the results are shown in Figure 7. The as-received AO-70 powder was crystalline and had the melting temperature at around 82 °C. After the as-received AO-70 was heated to 120 °C and quenched to -50 °C with a rate of 10 °C/min, amorphous AO-70 with a T_g at around 7 °C was obtained (Figure 7(a)). In PVAO hybrids (Figure 7(b)), the shift of the only T_g , attributed to the T_g of PVAc, showed a similar variation trend with that of DMA results. Moreover, neither the melting peak nor glass transition peak of AO-70 was observed in the hybrids, indicating that AO-70 was miscible with PVAc in all hybrids.

Table 3 gives a summary of the T_g in terms of T_{gm} and the width of T_g denoted by $\Delta W_{T_g} = T_{gf} - T_{gi}$ for PVAO hybrids, where T_{gi} , T_{gm} , T_{gf} represent the onset, middle and end point of the glass transition region and the value of ΔW_{T_g} is related to the extent of composition fluctuations and dynamic heterogeneity in miscible blends [38].

The ΔW_{T_g} of the hybrids were higher than that of pure PVAc, which indicated the bigger dynamic heterogeneity of the hybrids with the adding of AO-70. Meanwhile, for the hybrids, the ΔW_{T_g} decreased first followed by the gradual increase with increasing the amount of AO-70. As strong intermolecular associations (H-bonds) between the components have been found to suppress concentration fluctuations and couple partially (at least) the segmental motions of the two components [39-41], PVAO-25 phr, whose ΔW_{T_g} value was the lowest, might have the strongest H-bonds or H-bond networks and lowest dynamic heterogeneity of AO-70 in PVAc matrix.

Table 3. Summary of the thermal properties of PVAO hybrids.

Sample name	T_{gm} (°C)	T_{gi} (°C)	T_{gr} (°C)	Δw_{Tg} (°C)
PVAO-0 phr	39.82	36.54	42.32	5.78
PVAO-6.25 phr	31.92	29.02	37.09	8.07
PVAO-12.5 phr	28.97	25.92	34.42	8.50
PVAO-25 phr	27.36	24.74	31.60	6.86
PVAO-37.5 phr	25.12	20.49	27.83	7.34
PVAO-50 phr	21.75	17.20	25.12	7.92

Figure 8 shows the XRD traces of AO-70 and PVAO hybrid. The as-received and amorphous AO-70 displayed typical crystalline and amorphous characteristics, respectively. For PVAO-50 phr, the trace was similar to that of pure PVAc and no crystalline features were detected in the hybrid, suggesting the existence of only the amorphous AO-70 in PVAO hybrids.

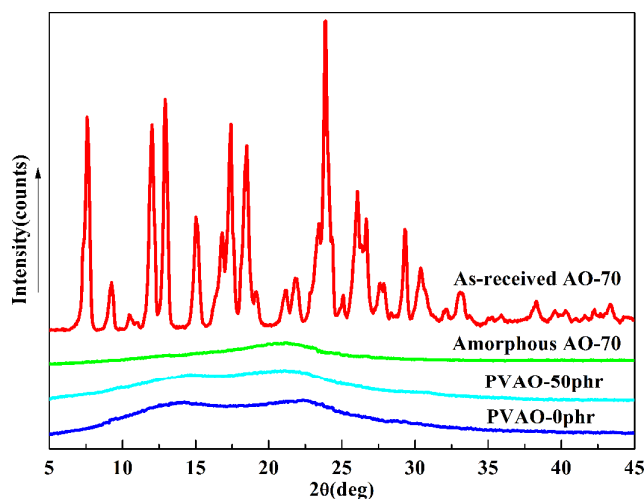


Figure 8. X-ray diffraction curves of AO-70 and PVAO hybrids.

3.4 Analysis of H-bonds in PVAO hybrids by MD simulation

Since only amorphous hindered phenol existed in PVAc, MD simulation based on an amorphous cell was used to obtain detailed quantitative information about H-bonds in PVAO hybrids. The simulation results of the pair correlation function, the number of H-bonds as well as the H-bond predominant binding energy and FFV in the optimized amorphous cell are shown below.

The pair correlation function $g(r)$, related to the probability of finding another atom at a distance r from a specific atom, has been widely applied in studying H-bonds. In general, the distances between atoms of 2.6-3.1, 3.1-5.0, and above 5.0 Å belong to H-bonds, strong vdw force, and weak vdw force, respectively [42]. Figure 3-S (in supporting information) presents the pair correlation function results of H (in AO-70) and O (in PVAc and AO-70) in the optimized amorphous cell of PVAO-25 phr. The peak of the correlation function of H and O lie in 2-3.2 Å, suggesting high probability

for the two atoms in the distance and form H-bonds interaction.

Table 4. Average number of H-bonds in different PVAO hybrids by MD simulation.

Sample name	PVAO-6.25 phr	PVAO-12.5 phr	PVAO-25 phr	PVAO-37.5 phr	PVAO-50 phr
No. of H-bonds(a)	1	2	4	4	7
No. of H-bonds(b)	0	0	1	2	2

Table 4 lists the average number of intramolecular and intermolecular H-bonds in different PVAO hybrids calculated from the optimized amorphous cells. Five repeated cells obtained by the repeated MD simulation condition were used to obtain the number of H-bonds in those cells, and then the average number of H-bonds in different hybrids was obtained. The numbers of H-bonds (a) and (b) both increased with increasing the amount of AO-70 and the number of H-bonds (a) was larger than that of H-bonds (b) in all hybrids, indicating that H-bonds (a) were easier to form and play a more important role in hybrids. Meanwhile, the H-bonds (b) were not detected in PVAO-6.25 and 12.5 phr, which was consistent with that of 2D IR results. Moreover, the H-bonds showed big changes from PVAO-25 phr to 50 phr, indicating the probability of achieving the percolation threshold corresponding to the H-bond network with increasing the amount of AO-70.

How well two components were mixed with each other could be reflected by binding energy (E_{binding}), which was defined as the negative of the intermolecular interaction energy (E_{inter}) between two components [43]. And E_{inter} could be evaluated by the total energy (E_{total}) of the mixture and those of the individual components in the

equilibrium state. Thus, the E_{binding} between AO-70 and PVAc could be determined as follows:

$$E_{\text{binding}} = -E_{\text{inter}} = -(E_{\text{total}} - E_{\text{AO-70}} - E_{\text{PVAc}}) \quad (2)$$

where E_{total} , $E_{\text{AO-70}}$ and E_{PVAc} are the total energy of the PVAO hybrid, AO-70 and PVAc, respectively. E_{PVAc} is a constant (-2215.03 kcal/mol) because the number of PVAc chains were fixed in the amorphous cell.

Table 5. Binding energies of PVAO hybrids with different AO-70 amounts.

Sample name	E_{total} (Kcal/mol)	$E_{\text{AO-70}}$ (Kcal/mol)	E_{binding} (Kcal/mol)
PVAO-6.25 phr	-2571.40	-243.59	112.78
PVAO-12.5 phr	-2686.11	-325.56	145.52
PVAO-25 phr	-2944.44	-653.19	76.22
PVAO-37.5 phr	-3268.63	-978.43	75.17
PVAO-50 phr	-3486.01	-1226.77	44.21

The binding energies of PVAO hybrids are shown in Table 5. Negative E_{total} values indicated that the interaction between PVAc and AO-70 was favorable towards lower energy, therefore, the hybrids were stable. With increasing the amount of AO-70, the E_{binding} increased first followed by a decrease and reached the maximum value at 12.5 phr and the minimum value at 50 phr, indicating the best and worst mixing between AO-70 and PVAc due to the variation of H-bonds in PVAO-12.5 phr and PVAO-50 phr, respectively. Moreover, H-bonds between AO-70 and PVAc were more stable than that with AO-70.

According to the Williams-Landel-Ferry (WLF) equation based on the free volume theory [44], FFV, which was commonly used to characterize the efficiency of chain packing and the amount of free space in a polymer matrix, was greatly affected by H-bonds and in turn affected the damping properties. A common definition of FFV was:

$$FFV = \frac{V - V^*}{V} \quad (3)$$

where V and V^* are the specific volume and occupied volume, respectively.

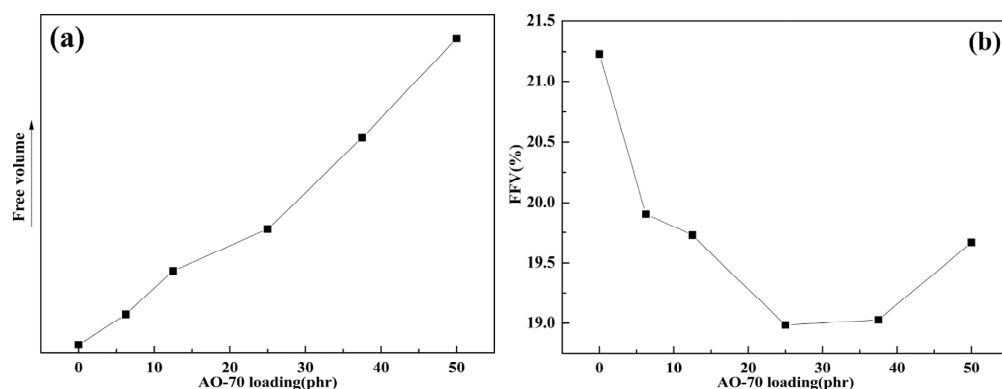


Figure 9. (a) Free volume and (b) Fractional free volume of PVAO hybrids calculated by MD simulation.

Figure 9 depicted the free volume and FFV results of PVAO hybrids calculated by MD simulation. With increasing the amount of AO-70, the FFV decreased first and reached a minimum value at PVAO-25 phr due to the most perfect H-bond network in PVAO-25 phr, and then a great increase occurred at PVAO-50 phr, which was attributed to the destruction of the H-bond network.

According to the above quantitative analysis and experiment results, a detailed analysis on the synergy effects of relevant influencing factors on the damping

mechanism of PVAO hybrids could be put forward. For PVAO-6.25 phr and 12.5 phr, the rapid increase of the damping properties was mainly attributed to the intermolecular H-bonds between PVAc and AO-70 and the H-bond predominant binding energy between them. Besides the intermolecular H-bonds, the rapid increase of the damping property for PVAO-25 phr could be mainly attributed to the most perfect H-bond network, resulting in the relatively most compact chain packing in the hybrid, which made more friction energy dissipation. PVAO-37.5 phr did not show obvious improvement in the damping property, compared with that of PVAO-25 phr, though the number of intramolecular H-bonds in PVAO-37.5 phr was larger than that of PVAO-25 phr while other factors were almost the same, indicating that intramolecular H-bonds in AO-70 had little effects on the damping property of the hybrids. For PVAO-50 phr, Even though the number of intermolecular H-bonds was largest, the damping property showed a slight improvement, because the largest amount of AO-70 led to the relatively high FFV and lowest binding energy in PVAO-50 phr, which caused less friction energy dissipation.

4 Conclusions

The fundamental mechanism of the improved damping property of PVAc contributed by the introduction of AO-70 was systematically elucidated by the combination of experiment and MD simulation. Since AO-70 and PVAc could form both intra- and intermolecular H-bonds, the intermolecular H-bonds combined with its predominant binding energy and FFV as well as the perfect H-bond network was the main attribution to the improvement of the damping properties. Whereas the

intramolecular H-bonds had little or negative effects on the damping properties and the destruction of the H-bond network also had negative influences on the damping properties of the hybrids.

Therefore, it is indicated that there was an optimum ratio of AO-70 to PVAc for achieving the proper damping property. And these fundamental studies are expected to provide some useful information to design and fabricate the high-performance polymeric damping materials.

ACKNOWLEDGEMENTS

Financial supports of the National Natural Science Foundation of China (51273132, 51227802 and 51121001) and Program for New Century Excellent Talents in University (NCET-13-0392) are gratefully acknowledged.

REFERENCES

- [1] Gusev AA, Feldman K, Guseva O. *Macromolecules* 2010, **43**, 2638-2641.
- [2] Sperling LH. *John Wiley & Sons*: 2005.
- [3] de Gennes P-G. *J. Chem. Phys.* 1971, **55**, 572-579.
- [4] Sperling L, Fay J. *Polym. Advan. Technol.* 1991, **2**, 49-56.
- [5] Fradkin D, Foster J, Sperling L, Thomas D. *Polym. Eng. Sci.* 1986, **26**, 730-735.
- [6] Maekawa M, Nitta M, Kako C, *In Soc Auto Eng Jpn* 1990, **44**, 49, CAS.

- [7] Thomas S, George A. *Eur. Polym. J.* 1992, **28**, 1451-1458.
- [8] Li F, Hasjim J, Larock RC. *J. Appl. Polym. Sci.* 2003, **90**, 1830-1838.
- [9] Qin C-L, Cai W-M, Cai J, Tang D-Y, Zhang J-S, Qin M. *Mater. Chem. Phys.* 2004, **85**, 402-409.
- [10] Qin C, Zhao D, Bai X, Zhang X, Zhang B, Jin Z, et al. *Mater. Chem. Phys.* 2006, **97**, 517-524.
- [11] Wu C, Yamagishi TA, Nakamoto Y, Ishida SI, Kubota S, Nitta KH. *J. Polym. Sci. B. Polym. Phys.* 2000, **38**, 1496-1503.
- [12] Wu C, Akiyama S. *J. Polym. Sci. B. Polym. Phys.* 2004, **42**, 209-215.
- [13] Liu Q, Zhang H, Yan X. *Iran. Polym. J.* 2009, **18**, 401-413.
- [14] Kaneko H, Inoue K, Tominaga Y, Asai S, Sumita M. *Mater. Lett.* 2002, **52**, 96-99.
- [15] Gao Y, Wang X, Liu M, Xi X, Zhang X, Jia D. *Mater. Design.* 2014, **58**, 316-323.
- [16] Qiao B, Zhao X, Yue D, Zhang L, Wu S. *J. Mater. Chem.* 2012, **22**, 12339-12348.
- [17] Song M, Zhao X, Li Y, Hu S, Zhang L, Wu S. *RSC Adv.* 2014, **4**, 6719-6729.
- [18] Cho M. *Chem. Rev.* 2008, **108**, 1331-1418.
- [19] Woutersen S, Hamm P. *J. Phys-condens. Mat.* 2002, **14**, R1035-R1062.
- [20] Fayer M. *Annu. Rev. Phys. Chem.* 2009, **60**, 21-38.
- [21] Kim YS, Hochstrasser RM. *J. Phys. Chem. B* 2009, **113**, 8231-8251.
- [22] Zhuang W, Hayashi T, Mukamel S. *Angew. Chem. Int. Edit.* 2009, **48**, 3750-3781.
- [23] Tamai Y, Tanaka H, Nakanishi K. *Macromolecules* 1996, **29**, 6750-6760.
- [24] Tamai Y, Tanaka H, Nakanishi K. *Macromolecules* 1996, **29**, 6761-6769.

- [25] Noda I, Dowrey A, Marcott C, Story G, Ozaki Y. *Appl. Spectrosc.* 2000, **54**, 236A-248A.
- [26] Noda I. *Vib. Spectrosc.* 2004, **36**, 143-165.
- [27] Wu Y, Jiang J-H, Ozaki Y. *J. Phys. Chem. A* 2002, **106**, 2422-2429.
- [28] Amari T, Ozaki Y. *Macromolecules* 2002, **35**, 8020-8028.
- [29] Alexiadis O, Mavrantzas VG. *Macromolecules* 2013, **46**, 2450-2467.
- [30] Huang J, Häussinger D, Gellrich U, Seiche W, Breit B, Meuwly M. *J. Phys. Chem. B* 2012, **116**, 14406-14415.
- [31] Pagliai M, Muniz-Miranda F, Cardini G, Righini R, Schettino V. *J. Phys. Chem. Lett.* 2010, **1**, 2951-2955.
- [32] Wang Z, Whitby RL, Rousseau M, Nevill S, Geaves G, Mikhalovsky SV. *J. Mater. Chem.* 2011, **21**, 4150-4155.
- [33] Sun H. *J. Phys. Chem. B* 1998, **102**, 7338-7364.
- [34] Zhu S, Yan L, Zhang D, Feng Q. *Polymer* 2011, **52**, 881-892.
- [35] Khalili M, Liwo A, Jagielska A, Scheraga HA. *J. Phys. Chem. B* 2005, **109**, 13798-13810.
- [36] Spyriouni T, Vergelati C. *Macromolecules* 2001, **34**, 5306-5316.
- [37] Wu P, Yang Y, Siesler H. *Polymer* 2001, **42**, 10181-10186.
- [38] Yang Z, Han CD. *Macromolecules* 2008, **41**, 2104-2118.
- [39] Masser KA, Runt J, editors. *Macromol. Symp.* 2009; Wiley Online Library: 2009; 221-227.
- [40] Zhang S, Casalini R, Runt J, Roland C. *Macromolecules* 2003, **36**, 9917-9923.

- [41] Fragiadakis D, Runt J. *Macromolecules* 2009, **43**, 1028-1034.
- [42] Ma X, Zhu W, Xiao J, Xiao H. *J. Hazard. Mater.* 2008, **156**, 201-207.
- [43] Solimannejad M, Alkorta I. *J. Phys. Chem. A* 2006, **110**, 10817-10821.
- [44] Wu C. *Polymer* 2010, **51**, 4452-4460.

Molecular insights into the damping mechanism of Poly(vinyl acetate)/hindered phenol hybrids by a combination of experiment and molecular dynamics simulation

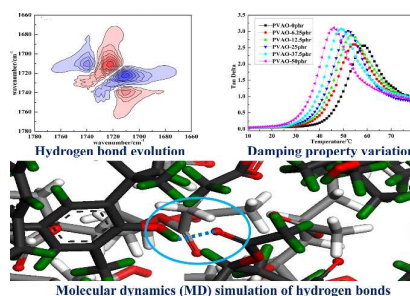
Kangming Xu, Fengshun Zhang, Xianlong Zhang, Jiwei Guo, Hong Wu*,
Shaoyun Guo*

State Key Laboratory of Polymer Materials Engineering, Polymer Research Institute of Sichuan University, Chengdu, Sichuan, 610065, China

*E-mail: wh@scu.edu.cn (Hong Wu); nic7702@scu.edu.cn (Shaoyun Guo).

Tel./Fax: +86-028-85406077 (Hong Wu); +86-028-85405135 (Shaoyun Guo)

Graphical abstract with text



By combining experiment and MD simulation, the relationship between hydrogen bond evolution and damping property variation of PVAc was revealed.